Effect of Metal Oxide additions to Quality of Ge/GeO_2 interfaces

Hongfei Li, John Robertson

Engineering Dept, Cambridge University, Cambridge CB2 1PZ, UK

Abstract

Alloying amorphous GeO_2 with Y2O3 and related group IIIA oxides has been found experimentally to improve its properties as a gate dielectric in field effect transistors. The mechanism of this is studied by density functional calculations. The metal coordination is found to be 6-7, by an increase of the oxygen coordination to 3. The alloying is found to increase the bulk modulus. Alloying also increases the formation energy of the oxygen vacancies in GeO_2 next to the metal sites. Alloying also increases the vacancy formation energy of oxygens that are second neighbours of the metal sites. In this way, a relatively small metal concentration can reduce the O vacancy diffusion rate and thereby the GeO evolution rate. Oxygen vacancies at the Ge/GeO_2 interface next to a metal site are found to divide into two types, those which rebond across the vacancy (La, Hf), and those without rebonding (Y, Sc, Al), the latter being preferable as they do not give rise to gap states.

Introduction

The continued scaling of CMOS devices will require the replacement of silicon channels with a higher mobility semiconductor such as Ge or InGaAs. Ge is the simpler option because both its electron and hole mobilities are much larger than those of Si [1-5]. However, its native oxide GeO_2 is much worse than SiO_2 and the Ge/GeO_2 interface displays a much larger interface state density, D_{it}, than the Si/SiO_2 case [1,4], for reasons that are not fully understood. It is known that the Ge/GeO_2 interface can be smooth and abrupt [6,7], just like the Si/SiO_2 interface. It can also in some cases have a low D_{it} [8]. One possible reason of the poor performance of GeO_2 is the greater stability of the Ge^{II} valence state of Ge and the higher volatility of the sub-oxide GeO molecule [9-11]. GeO_2 is also hygroscopic and soluble in water. A further problem is that while HfO_2 is compatible with Si and SiO_2, HfO_2 is less effective as a high K oxide on GeO_2 [2].

Recently, Lu et al [12-16] have noticed that alloying group IIIA oxides such as Y_2O_3 into GeO_2 can have a remedial effect. At a simple level, the oxide alloying raises the evolution temperature of GeO and reduces the aqueous dissolution rate of GeO_2 [13]. It also lowers the D_{it} and increases the reliability of GeO_2 based gate stacks. The evolution of GeO is known to occur by the diffusion of oxygen vacancies through the GeO_2 layer from the Ge/GeO_2 interfaces to the GeO_2 surface, where evolution occurs [11]. Thus, reduced GeO evolution must occur by an effect on O vacancies. Multilayer stacks with the Y_2O_3 alloyed layer at the top or the bottom both raised the GeO evolution temperature by a similar amount [12], so this shows that O vacancy transport across the oxide layer is impeded. Nevertheless these effects occur at quite small alloying fractions [14], so the mechanism must be clearly identified. In addition, the metal oxides were not all uniformly beneficial; some improved the water etching

rate, but some led to an increase in D_{it} [15]. There have been various attempts to design gate stacks that avoid the problems of GeO_2 [17-22], the alternative is to try to improve it.

This indicates that it is useful to understand the processes within alloyed GeO_2 at a more atomic scale. We use supercell models to calculate the effect of alloying on the oxygen vacancies in the bulk, on oxygen vacancies at the Ge/GeO_2 interface, and on whether the vacancies lead to states within the Ge band gap energy range.

Method.

The calculations are carried out using the plane wave density functional theory (DFT) code CASTEP [23], using ultrasoft pseudopotentials and a plane wave cutoff of 400 eV. This converges the energies to under 0.01 eV per atom. The DFT energetics are corrected by a van der Waals term, as in the scheme of Grimme [24,25]. Band gap and defect level calculations employ the screened exchange method [26] to correct the DFT band gap error.

We generate a 144 atom random network supercell of GeO_2 by DFT molecular dynamics, for reference. We then generated a smaller 72 atom supercell of GeO_2 for the alloying studies. To form the alloy models, we replace pairs of Ge's with trivalent Y, La, Sc, Lu or Al atoms. It is necessary to also remove one oxygen per pair of metal atoms to keep valence balance. An important point is that the coordination numbers of the Sc, Y and La metal atoms are much larger than those of Ge, so a good alloy structure requires careful relaxation so that the system is not trapped in a metastable minimum of a substituted network. Instead, a short molecular dynamics run is first applied, followed by energy minimization. It was found necessary to use metal pseudopotentials containing semi-core levels to obtain a good atomic volume of Y_2O_3. The calculations of electronic structure were carried out using the screened exchange density functional [26] to correct the band gap error of simple DFT. Norm conserving pseudopotentials are used for this step.

Results

Bulk sites and Bulk defects

Fig. 1(a) shows the supercell of the random network of GeO_2. All the Ge sites are 4-fold coordinated and all the O sites are 2-fold coordinated, just as in an a-SiO_2 network. Figs 1(b-d) show the networks containing 8%, 16% and 33% Y loading respectively, as a fraction of the cation sites. It is seen that the Y sites tend to be paired close by. The coordination numbers of the metal sites are given in Table 1, being 6.25 for Y sites. This is achieved by the Y atoms making additional bonds to oxygens, converting those oxygens into 3-fold sites.

The metals Sc, Y and La are highly electropositive atoms with large ionic radii. Fig. 2 shows the network structure of the 16% metal alloy for the three different trivalent metals. As the metal changes from Sc to Y to La, we see that the metal-O coordination increases with atomic number and ionic radius, as summarized in Table 1. Thus, there is some dependence of metal coordination on ionic radius. HfO_2 alloying is also included, in that case Hf is tetra-valent like Ge, so there is no need to remove an oxygen for valence balance.

Fig 3(a) plots the atomic volume per oxygen atom of the Y alloy as a function of the cation fraction. It is seen that Y addition causes a decrease in mean atomic volume below the linear interpolation line of Vegard's law, corresponding to a downward bowing. This is as expected for exothermic mixing. The exothermic mixing of Y_2O_3 and GeO_2 means that Y_2O_3 behaves like an oxide base towards GeO_2 [27-29]. This is because of the large Y ionic radius.

Lu and Toriumi [14] proposed that various features of electrical reliability might arise from an increase in rigidity of the bonding network, which reduces the rate of defect formation. We therefore calculated the bulk modulus of the oxide alloys as a function of metal content. Fig. 3(b) shows that the bulk modulus increases progressively with Y addition up to 50% metal. We also calculated the bulk modulus of crystalline (hexagonal) Y_2O_3 and pyrochlore $Y_2Ge_2O_7$, for reference. We see that the amorphous phases have much lower bulk moduli than the crystalline phase of the same composition.

Oxygen Vacancies

We now consider the oxygen vacancies. Fig. 4(a) shows that the neutral O vacancy in pure GeO_2 relaxes and reconstructs to form a Ge-Ge bond. This behavior is like the O vacancy in SiO_2 [30]. The Ge-Ge bond gives rise to gap states, as seen in the sX partial density of states in Fig 5(a), with a filled bonding state at 0.8 eV above the bulk valence band maximum (VBM) at 0 eV and an empty antibonding state at +6.8 eV, that is just above the conduction band minimum given a GeO_2 band gap of 6.2 eV. The formation energy of the relaxed O vacancy in a-GeO_2 is about 3.33 eV, Table 2. Clearly this energy forms a distribution, due to disorder, but its energy range is not so large, as the coordination does not vary.

We then calculated the formation energy for the neutral O vacancy in the GeY_xO_y alloys for different compositions. There are three different O vacancy sites in the GeY_xO_y alloys as shown in Fig4(b), (i) an O bonded to two Y and one Ge, (ii) an O bonded to one Y and two Ge's, and (iii) an O bonded to one Y and one Ge. The fraction of type (iii) sites declines to 0% at about 33% Y content.

Figs 4(c-e) show the relaxed geometries of these three vacancy sites. We see that vacancies (i) and (iii) relax their bond angles, but there is no reconstruction or rebonding across the vacancy for Y. In contrast, for vacancy (ii), the two Ge dangling bonds rebond into a Ge-Ge bond, just as in the case of the O vacancy in GeO_2 itself.

Table 2 shows the defect formation energies for these relaxed vacancies next to Y sites, in the 8% Y network, which are 4.27 eV, 4.67 eV and 3.04 eV for vacancies (i), (ii) and (iii), respectively. This is roughly in line with the number of bonds broken to create the vacancy. Note that the largest formation energy is for vacancy (ii) with two adjacent Ge sites, *despite* 'getting energy back' for reforming the Ge-Ge bond. The calculation is for an O chemical potential of 0 eV, that is assuming the removed O atoms form O_2 molecules. Thus, on average, there is a substantial 0.66 eV average increase in the O vacancy formation energy in GeO_2 by adding the Y. This average is also consistent with the average O vacancy formation that we calculate for O sites in the pyrochlore $Y_2Ge_2O_7$ crystal. The O vacancy formation energy in $Y_2Ge_2O_7$ at its three different sites is 4.29 eV, 4.92 eV and 4.29 eV, or 4.50 eV on

average. The average formation energy increases with increased alloying, because the fraction of Vo3 sites goes down.

Superficially, the calculated 0.66 eV average increase in vacancy formation energy at O sites adjacent to Y sites partly explains the reduced molecular GeO evolution rate in the alloys. However, the data shows that the rise in evolution temperature occurs already in alloys with only 10% Y [13]. This Y addition would only affect vacancies at 30% of oxygen sites (assuming 3-coordinated oxygens). A percolation path for O diffusion along O sites would not be blocked as it is below the roughly 55% percolation threshold for this lattice.

Thus, we also calculated the vacancy formation energy at O sites that are second nearest neighbors to Y sites, Fig 4(f). We found the O vacancy formation energy increased from 3.33 eV for pure GeO_2 to 3.44 eV for the second neighbor sites, a moderate increase. An effect at the second neighbor distance increase the effect's range by a factor of roughly three over the nearest neighbor effect, of the Y-O bond length, or roughly 9 times in terms of projected area, as illustrated in Fig 4(f). Now the addition of 10% Y will have a full blocking effect on O vacancy diffusion, by percolation, consistent with experimental observations.

We now consider the electronic structure of the vacancies. Fig 5(b-d) shows the calculated partial density of states on atoms at the three different vacancy sites, V_{O1}, V_{O2}, V_{O3}. For Vo1), the single Ge dangling bond (DB) gives rise to a filled state for a negative DB lying at -0.2 eV just below the top of the valence band. On the other hand, the Y sites adjacent to the vacancy give rise to no gap states, their PDOS starts at 3.3 eV and above. In effect they form positive Y dangling bond states in the conduction band. For Vo2, the Ge-Ge re-bond gives rise to a filled bonding state in the valence band, and an antibonding state at +1.7 eV in the Ge conduction band, and no gap states. In Vo3, again the Ge DB site next to the vacancy gives rise to a filled defect state at 0 eV, at the top of the valence band.

We also calculated the O vacancy formation energy as a function of metal. Limiting ourselves to the vacancy V_{O1}, we see that its structure depends on the metal, as shown in Fig 6. The formation energy increases from Sc to Y, but it then decreases for La. This is because the large ionic radius of La allows an extra La-O bond to form across the vacancy (circled), and this decreases the formation energy (Table 3). The Ge dangling bond atoms are shown in bright green in these figures.

Interfacial Defects

We now consider some possible disadvantages of metal addition, by calculating the effects on O vacancies at the Ge/GeO_2 interface. We saw from fig 6(b) that an O vacancy at the Ge/GeO_2 does not form gap states in its simple configuration. The main question is whether O vacancies between a metal atom and the Ge side will form gap states. Generally this will occur if a metal-Ge bond forms [19-21].

We construct a Ge/GeO_2 interface model with 48 Ge atoms in 6 layers, a (100) interface, 36 formula units of amorphous GeO_2, and terminated on both top and bottom by hydrogens, with 15Å of vacuum. The Ge sites on the Ge side of the interface each have two dangling bonds

pointed towards the GeO_2 side. One of these at each site forms a Ge-O-Ge bridge with an adjacent Ge parallel to the interface, leaving the remaining DB to form a Ge-O bond across to the GeO_2, as in the Yu and Tersoff [33] model. This is the basic interface structure. We then replace a Ge site within one O of the interface by a metal atom. An additional H atom is added to the GeO_2 side if the metal atom is trivalent, for valence balance.

An oxygen atom between the metal atom and the Ge interface atom is then removed to make the vacancy, and the structure allowed to relax. Fig 6(a-d) shows the structures of the relaxed interfacial O vacancy for the different MGeOx/Ge interfaces. We see that a metal-Ge bond does not form in the cases of Sc, Y and Al, but it does form in the cases of La and Hf. This is slightly different to that found previously by Dimoulas [21]. For Hf, it is similar to that found in previously [31]. There is a clear gap state at +1 eV for the Hf case. These results can be summarised in a plot of ionic radius vs reactivity, as previously [16], Fig 9. Thus, the reactivity of Ge with the metal to form a germanide corresponds to its ability to form a Ge-metal bond across the vacancy. It is interesting that there is subtle dependence of this energy on the ionic radius of the group IIIA metal, so that Sc or Y are favored by not forming a bond, while La is too large and reactive.

Summary

Alloying oxides of electropositive metals into GeO_2 has a strong effect. The group IIIA metal oxides have a network modifying effect, increasing the coordination number of the oxygen atoms. The metal ion coordination is calculated to lie in the range 6-8. The alloying increases the bulk modulus of the alloys. Alloying generally increases the average formation energy of O vacancies over its value in pure GeO_2. This decreases the O diffusion which occurs via network oxygen sites, and thus reduces the volatility of GeO suboxide molecules. The alloying has an effect even at the second neighbor oxygens, accounting for the ability to reduce diffusion rates even at relatively low alloying fractions. For an oxygen vacancy at the Ge/GeO_2 interface where the vacancy might be bonded to a Ge and a metal ion in the oxide alloy, the effect varies with the metal. For the metals Sc, Y and Al, there is no rebonding across the vacancy, and this means that the defect makes no gap state. However, Hf and La bond have rebonding, and this gives rise to electrically active states near the Ge gap.

We acknowledge funding from EPSRC.

1. S Takagi, Tech Digest IEDM (2012) p23.1; S Takagi, R Zhang, J Suh, S H Kim, S H Kim, M Yokohama, K Nishi, M Takenaka, Jpn J Appl Phys **54** 06FA01 (2015)
2. Y Kamata, Materials Today 11 30 (2008)
3. J Robertson, R M Wallace, Mat Sci Eng R **88** 1 (2015)
4. A Toriumi, C H Lee, S K Wang, T Tabata, M Yoshida, D D Zhao, T Nishimura, K Kita, K Nagashio, Tech Digest IEDM (IEEE, 2011) p28.4
5. D Kuzum, A J Pethe, Y Oshima, P C McIntyre, K C Saraswat, Tech Digesr IEDM (IEEE, 2007) p723
6. T Sasada, Y Nakakita, M Takenaka, S Takagi, J App Phys **106** 073716 (2009)
7. R Zhang, P C Huang, J C Liu, M Takenaka, S Takagi, App Phys Lett **105** 081603 (2013)
8. A Delabie, F Bellenger, M Houssa, T Conard, S V Elshocht, M Caymax, M Heyns, M Meuris, App Phys Lett 91 082904 (2007)
9. K Kita,S Suzuki, H Nomura, T Takahashi, T Nishimura, A Toriumi, Jpn J App Phys **47** 2349 (2008)
10. S K Wang, K Kita, C H Lee, T Tabata, T Nishimura, K Nagashio, A Toriumi, J App Phys Phys **108** 054104 (2010)
11. S K Wang, K Kita, T Nishimura, K Nagashio, A Toriumi, Jpn J App Phys 50 04DA01 (2011)
12. C Lu, C H Lee, W Zhang, T Nishimura, K Nagashio, A Toriumi, Tech Digest SSDM (Fukuoka, 2013) B5-1.
13. C Lu, C H Lee, W Zhang, T Nishimura, K Nagashio, A Toriumi, App Phys Lett **104** 092909 (2014)
14. C Lu, A Toriumi, Tech Digest IEDM (IEEE, 2015) p14.6
15. C Lu, C H Lee, T Nishimura, K Nagashio, A Toriumi, App Phys Exp **8** 021301 (2015)
16. C Lu, C H Lee, W Zhang, T Nishimura, K Nagashio, A Toriumi, J Appl Phys **116** 174103 (2014)
17. R Zhang, T Iwasaki, N Takoa, M Takenaka, S Takagi, App Phys Lett **98** 112902 (2011) Ge/Al
18. L Zhang, H Li, Y Guo, K Tang, J Woicik, J Robertson, P C McIntyre, ACS Appl Mat Inter (2016)
19. E Simoen, J Mitard, G Hellings, G Eneman, B DeJaeger, L Witters, B Vincent, R Loo, A Delabie, S Sioncke, M Caymax, C Claeys, Mat Sci Semicon Proc **15** 588 (2012)
20. M Houssa, G Poutois, M Caymax, M M Heyns, App Phys Lett **92** 242101 (2008)
21. A Dimoulas, D Tsoutsou, Y Panayiotatos, A Sotiropoulos, G Mavrou, S F Galata, E Golias, App Phys Lett **96** 012902 (2010)
22. H Li, L Lin, J Robertson, App Phys Lett **101** 052903 (2012)
23. S J Clark, M D Segall, C J Pickard, P J Hasnip, M J Probert, K Refson, M C Payne, Z Krist **220,** 567 (2005)
24. S Grimme, J Comp. Chem, **27,** 1787-1799 (2006).
25. M Micoulat, L Cormier, G S Henderson, J Phys Cond Mat **18** R753 (2006)
26. S. J. Clark and J. Robertson, Phys. Rev. B **82**, 085208 (2010);
27. J J Liang, A Navrotsky, A Ludwig, J Mat Res **14** 11811 (1999)
28. G J Redhammer, G Roth, G Amthauer, Acta Cryst C **63** 193 (2007);
29. M Copel, N Bojarcuk, L F Edge, S Guha, App Phys Lett 97 182901 (2010)
30. E P O'Reilly and J Robertson, Phys Rev B **27** 3780(1983)
31. L Lin, K Xiong, J Robertson, App Phys Lett 97 242902 (2010)
32. K Xiong, P W Peacock, J Robertson, App Phys Lett **86** 012904(2004)
33. Y. Tu and J. Tersoff, Phys Rev Lett **89**, 086102 (2002).

Tables

Sc	Y	La
5.25	6.25	6.75

Table 1. Metal site coordination number in GeO_2.

Pure GeO_2	V1	V2	V3	V(2nn)
3.33	4.27	4.67	3.04	3.44

Table 2. Formation energy (eV) of the O vacancy in GeO_2 and the 3 types of oxygen vacancy in GeY_xO_2, in the O-rich limit, and of a bulk O vacancy that is a second neighbor of a Y site.

Sc	Y	La	Lu	Hf
3.47	3.77	3.61	3.74	4.69

Table 3. Formation energy (eV) of the V1 oxygen vacancy in $GeMe_xO_2$, in O-rich limit, as a function of the alloying metal (Me) oxide.

$GeSc_xO_2$	GeY_xO_2	$GeLa_xO_2$	$GeAl_xO_2$	$GeHf_xO_2$
2.95	2.55	2.51	3.45	3.37

Table 4. Formation energy of interfacial O vacancy for different metal additions.

Figure captions

1. Random network model of amorphous GeO_2. (b) network model of GeY_xO_2 with 8% Y, (c) with 16% Y and (d) with 33% Y. (green balls = Ge, red balls = O, blue balls = metal)
2. Random network models of $GeMe_xO_2$ with 16% metal, for Sc, Y, La, Lu and Hf doping, respectively. (green balls = Ge, red balls = O, blue balls = metal)
3. (a) Calculated atomic volume per O atom, vs Y doping ratio. (b) calculated bulk modulus of a-GeY_xO_2 compared to modulus of crystalline GeO_2, Y_2O_3 and $Y_2Ge_2O_7$.
4. GeO_2 network, containing relaxed O vacancy (Ge-Ge bond). (b) the three O sites in GeY_xO_2. (c-e) The relaxed geometries of the O vacancies at these 3 sites. Illustration of an O site that is a second neighbor to a O vacancy next to an Y atom. (green balls = Ge, red balls = O, blue balls = metal)
5. Calculated sX partial density of states (PDOS) of a Ge-Ge bond ion a-GeO_2. (b-d) calculated PDOS of atoms near the three O vacancies defined in fig 4.
6. Oxygen vacancies in GeO_2 alloyed with Sc, Y, La, Lu, and Hf oxide. Any Ge dangling bond site next to vacancy is shown as bright green.
7. Geometries of interfacial O vacancies and local PDOS of adjacent sites, for Sc, Y, La, Hf and Al oxide alloys on Ge. Note no bond reformaing for Sc, Y or Al.
8. Schematic of Lu/Toriumi diagram to show reactive/unreactive interfaces for metal oxide/GeO2 alloys on Ge, as defined against (experimental) electrical properties and ionic radii.

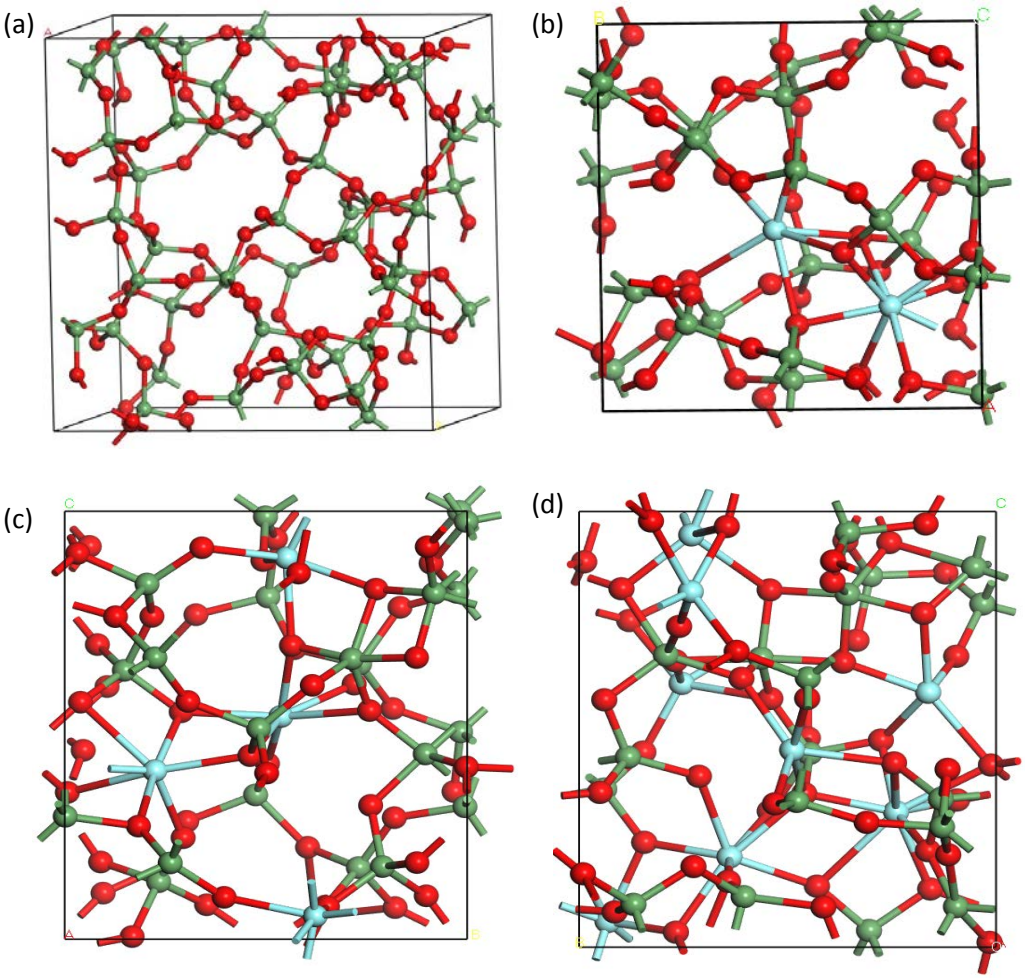

Fig. 1.

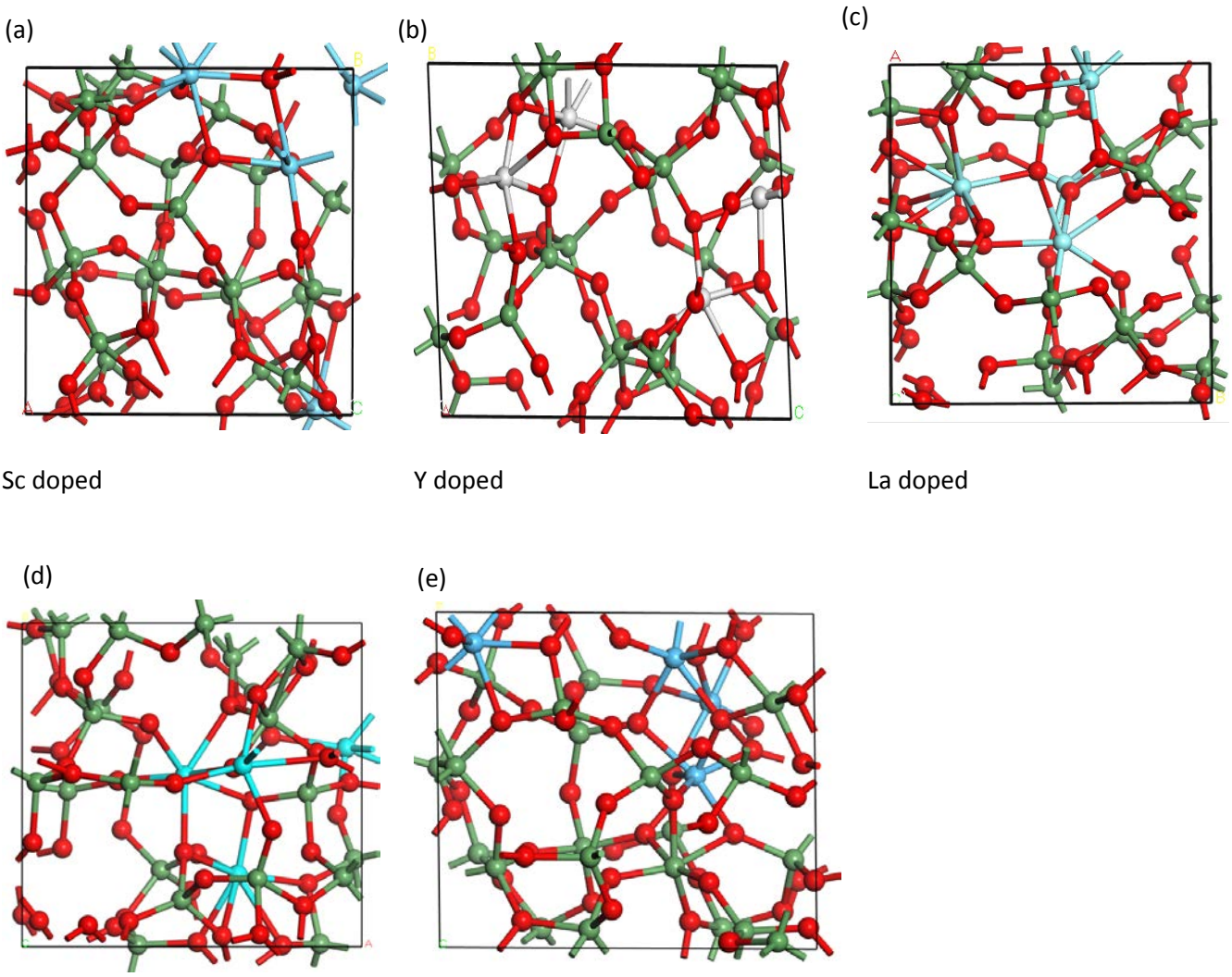

Fig 2.

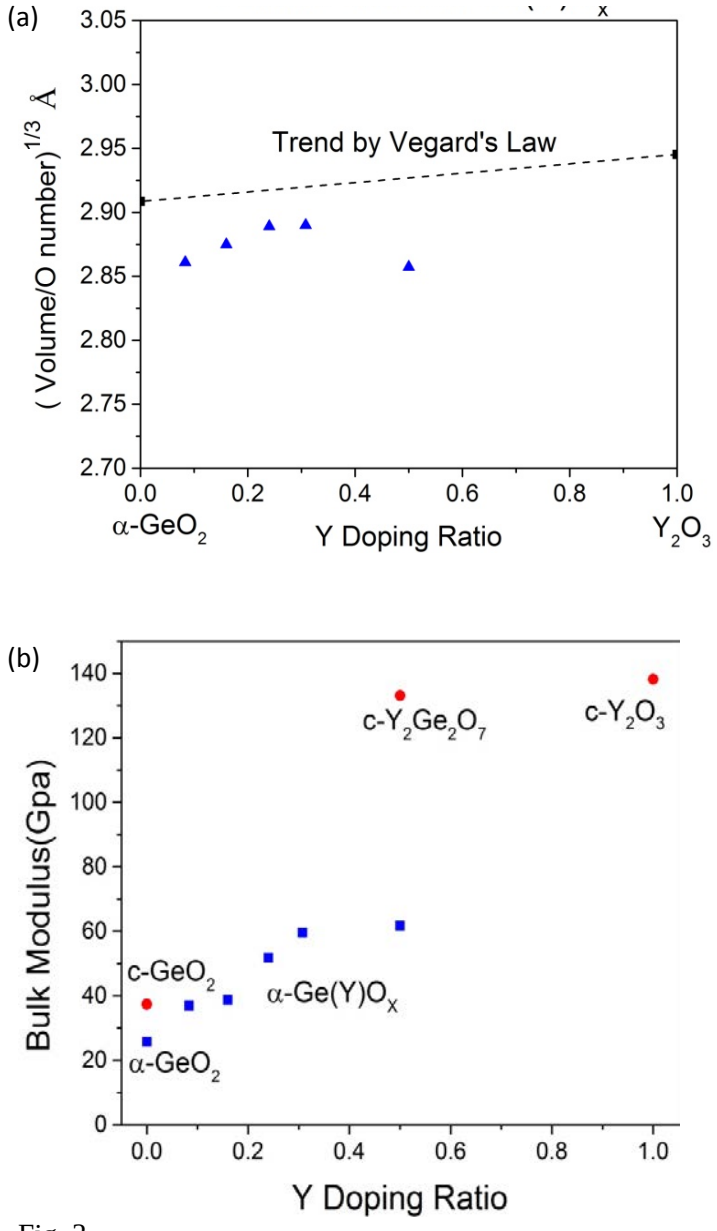
(a)
3.05
3.00
2.95
2.90
2.85
2.80
2.75
2.70
(Volume/O number)^1/3 Å
Trend by Vegard's Law
0.0
0.2
0.4
0.6
0.8
1.0
α-GeO2
Y Doping Ratio
Y2O3
(b)
140
120
100
80
60
40
20
0
Bulk Modulus(Gpa)
c-Y2Ge2O7
c-Y2O3
c-GeO2
α-Ge(Y)OX
α-GeO2
0.0
0.2
0.4
0.6
0.8
1.0
Y Doping Ratio

Fig. 3.

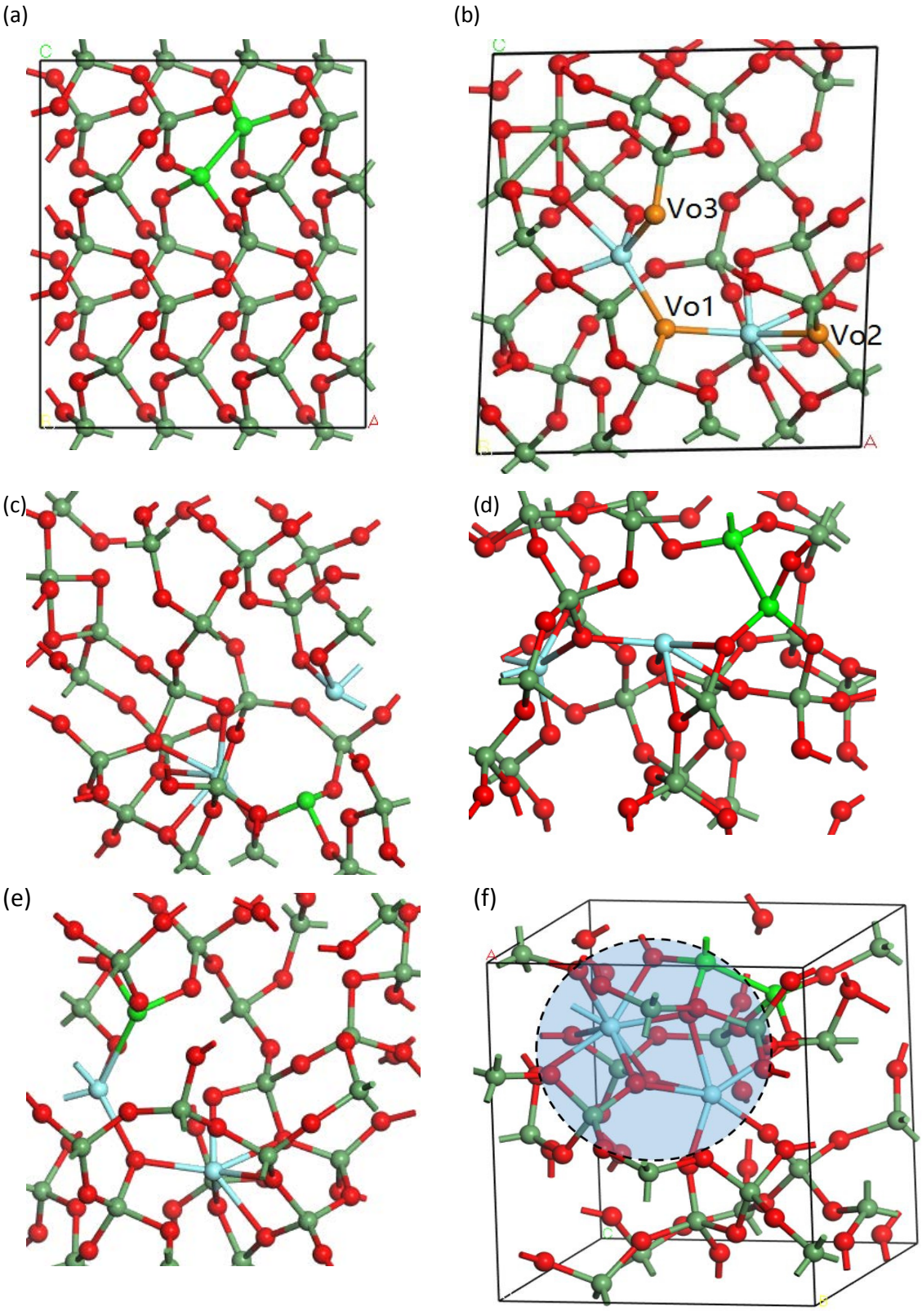

Fig. 4

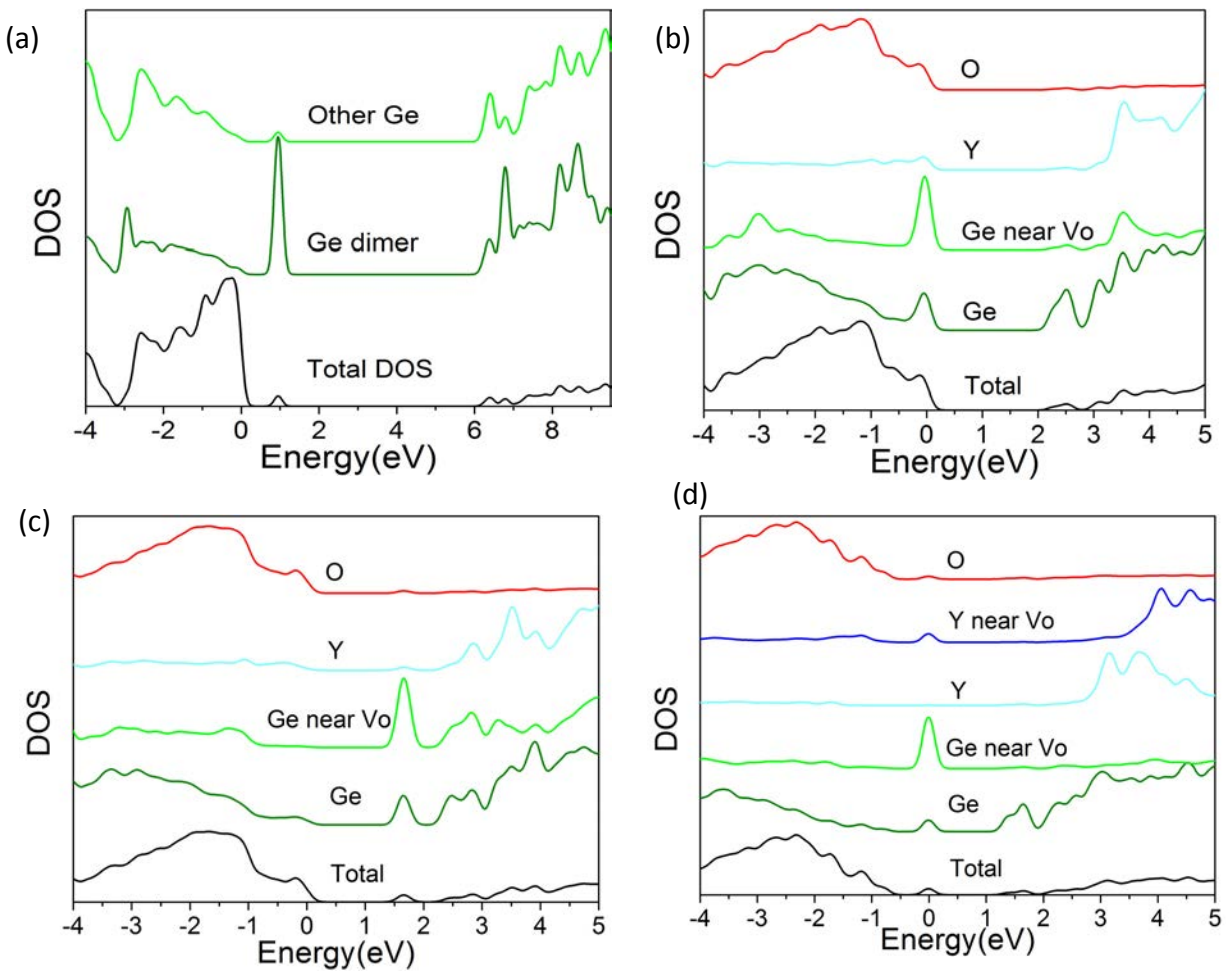
(a)
Other Ge
Ge dimer
Total DOS
DOS
Energy(eV)
(b)
O
Y
Ge near Vo
Ge
Total
DOS
Energy(eV)
(c)
O
Y
Ge near Vo
Ge
Total
DOS
Energy(eV)
(d)
O
Y near Vo
Y
Ge near Vo
Ge
Total
DOS
Energy(eV)

Fig. 5.

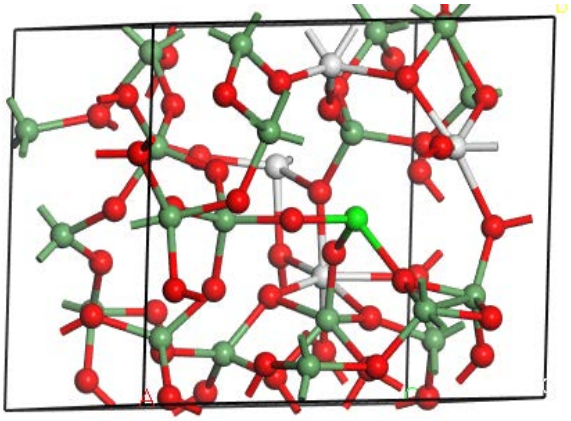

(a)

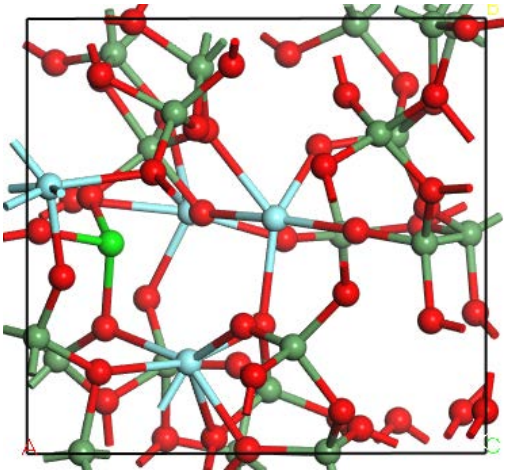

(b)

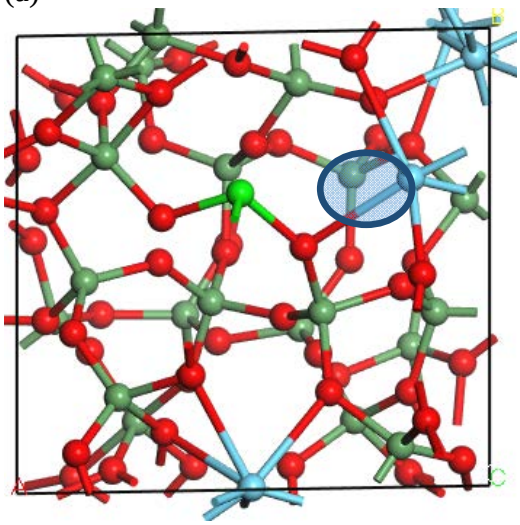

(c)

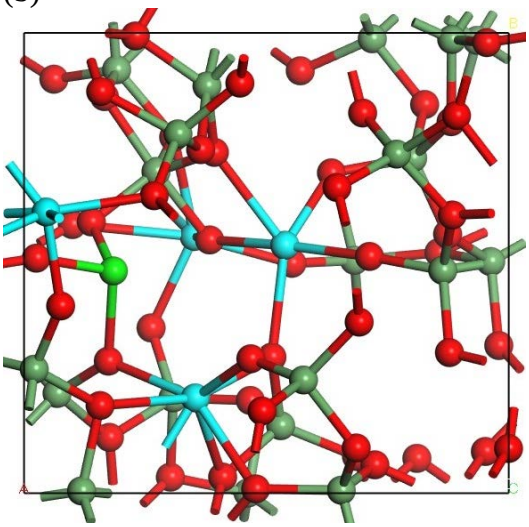

(d)

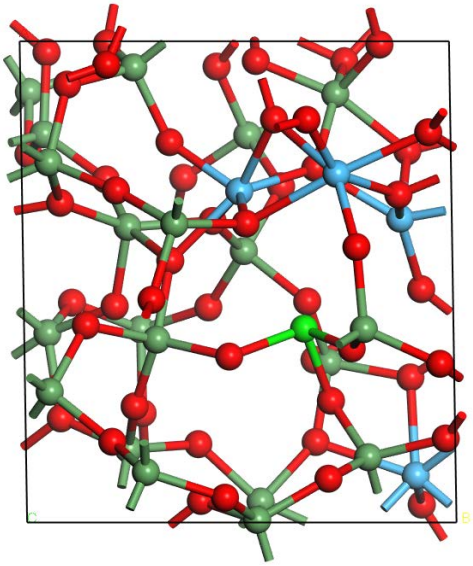

(e)

Fig. 6.

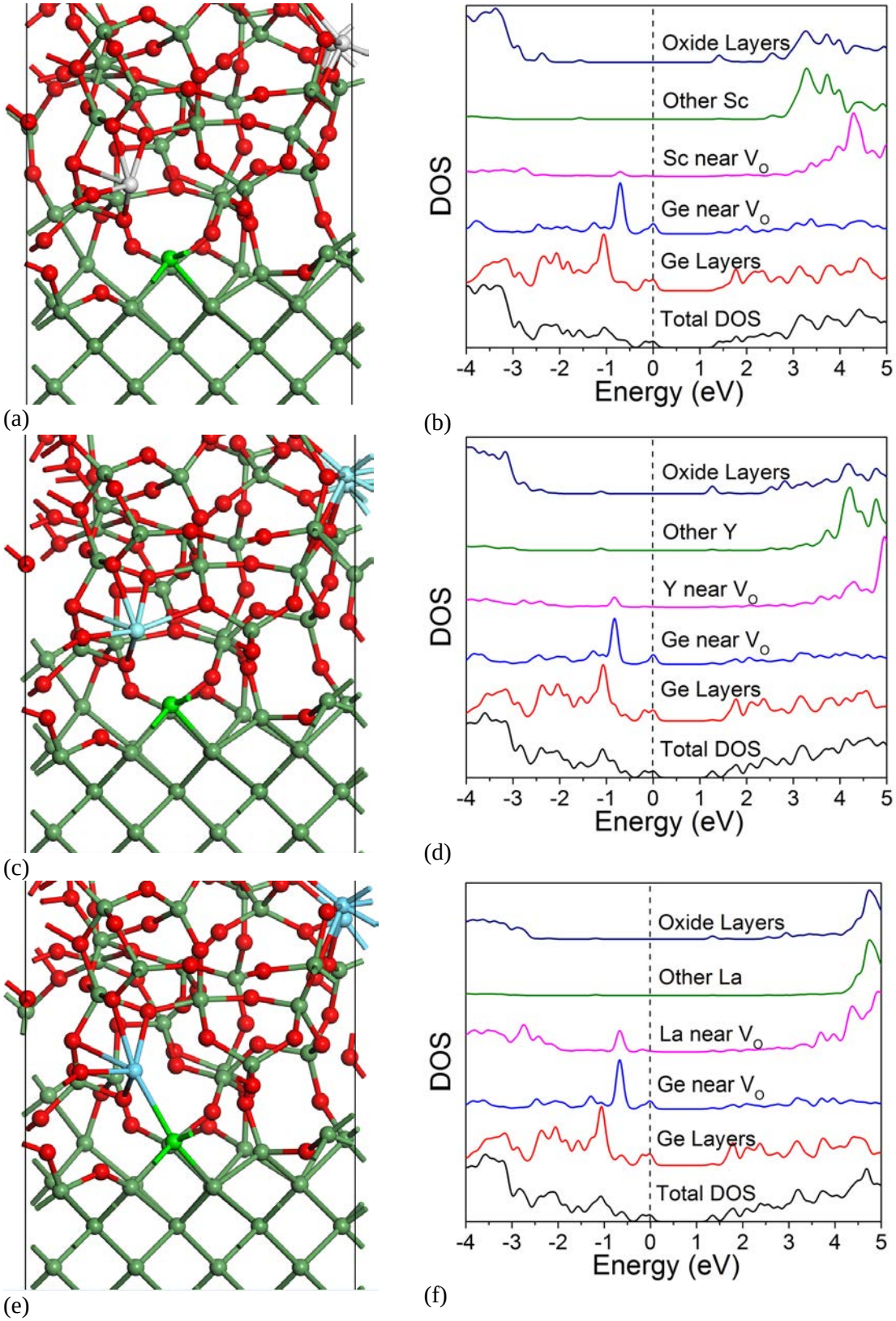
(a)
(b)
Oxide Layers
Other Sc
Sc near V$_O$
Ge near V$_O$
Ge Layers
Total DOS
DOS
-4 -3 -2 -1 0 1 2 3 4 5
Energy (eV)
(c)
(d)
Oxide Layers
Other Y
Y near V$_O$
Ge near V$_O$
Ge Layers
Total DOS
DOS
-4 -3 -2 -1 0 1 2 3 4 5
Energy (eV)
(e)
(f)
Oxide Layers
Other La
La near V$_O$
Ge near V$_O$
Ge Layers
Total DOS
DOS
-4 -3 -2 -1 0 1 2 3 4 5
Energy (eV)

Fig. 7.

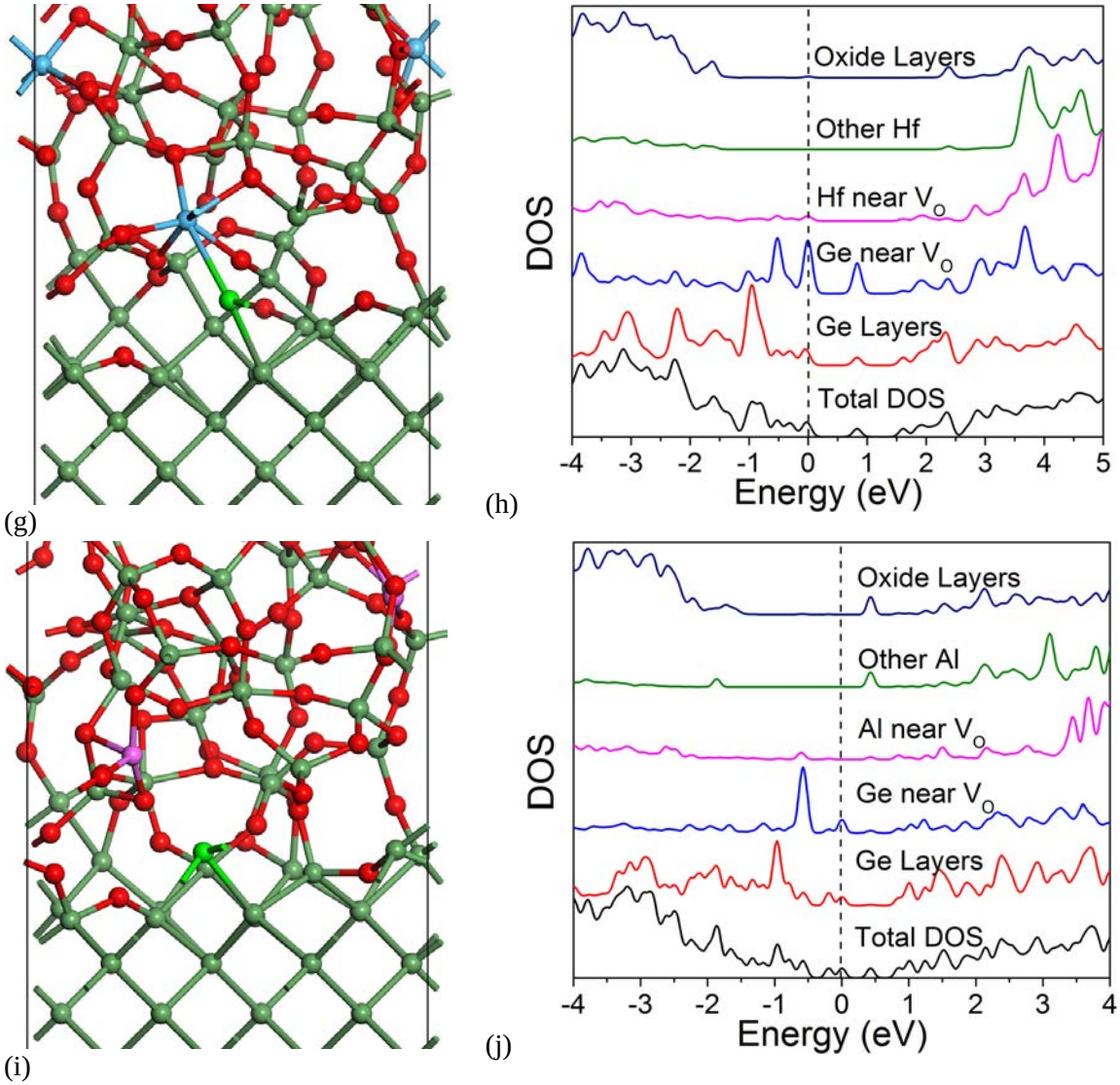
(g)
(h)
Oxide Layers
Other Hf
Hf near V_O
Ge near V_O
Ge Layers
Total DOS
DOS
-4 -3 -2 -1 0 1 2 3 4 5
Energy (eV)
(i)
(j)
Oxide Layers
Other Al
Al near V_O
Ge near V_O
Ge Layers
Total DOS
DOS
-4 -3 -2 -1 0 1 2 3 4
Energy (eV)

Fig. 7.

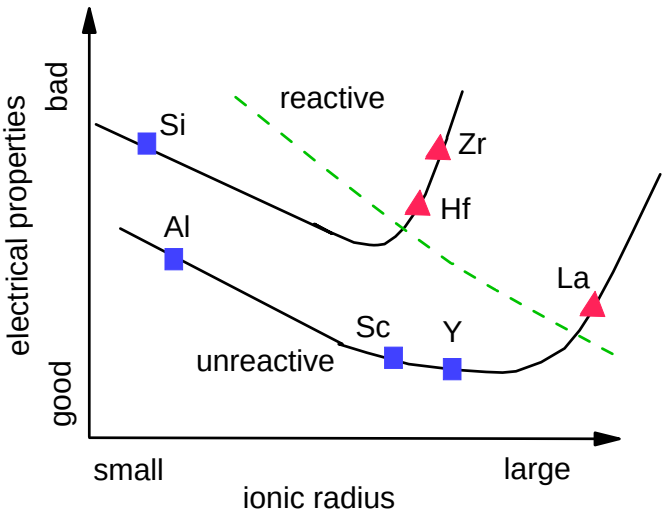
electrical properties
bad
good
reactive
Si
Zr
Hf
Al
La
Sc
Y
unreactive
small
large
ionic radius

Fig .8.